ChemComm

COMMUNICATION

View Article Online
View Journal | View Issue

Cite this: *Chem. Commun.*, 2022, 58, 9022

Received 10th May 2022,
Accepted 3rd July 2022

DOI: 10.1039/d2cc02649j

rsc.li/chemcomm

Formation of carotenoid supramolecular aggregates in nanocarriers monitored *via* aggregation-sensitive chiroptical output of enantiopure (3*S*,3′*S*)-astaxanthin†

Aleksandra Orlef, [a] Ewa Stanek, [b] Krzysztof Czamara, [b] Aleksandra Wajda [a] and Agnieszka Kaczor *[ab]

The aggregation-sensitive chiroptical (ECD and RROA) output, provided by enantiopure (3*S*,3′*S*)-astaxanthin, was used to investigate and control the assembling processes of the carotenoid in Pluronic F-127 nanoparticles. The process of carotenoid *J*-aggregation inside nanocarriers is interfered with by the formation of kinetically stabilized *H1* self-assemblies outside the micelles. Nanocarriers with encapsulated stable *J*-aggregates provide controlled release of carotenoid molecules to primary murine adipocytes.

Carotenoids are one of the most important nutrients showing a variety of positive health effects, including, confirmed in large cohort studies, reduction of cancer risk[1,2] and cardiovascular disease risk.[3] Recently, carotenoids have also gained attention due to adipocyte browning activity.[4,5] Browning of the adipose tissue, that is, the development of beige adipocytes in the white adipose tissue, significantly accelerates fat metabolism.[6] On the eve of the global diabetes epidemic, adipose tissue browning could be an efficient strategy to prevent obesity and related metabolic disorders.[6] As primarily accumulated in adipocytes, carotenoids appear as the archetypal browning agents.

However, carotenoids for use as dietary supplements encounter problems due to their low bioavailability and bioaccessibility arising from their low water solubility and sensitivity to environmental factors including light, oxygen, pH, and high temperatures. In the human body, after the liberation of carotenoids from the food matrix, they are solubilized into mixed micelles and in this form passed to enterocytes in the intestine.[7] Mixed micelles are efficient vehicles for carotenoids, providing their stabilization during transport. Therefore, to biomimic a natural solution, various artificial nanocarrier systems were proposed to encapsulate carotenoid molecules to increase their stability and efficient delivery.[8–12] Most studies on carotenoid-loaded nanocarriers typically characterize their stability, sizes, zeta potentials, encapsulation efficiencies, and release properties, yet not much is understood about the mechanisms of particle formation and carotenoid encapsulation. Although this problem was signaled about 20 years ago,[13] not much has changed and we have only a scarce understanding of carotenoid structures inside nanoparticles and associated aggregation processes that may have dramatic consequences on the solubilization of carotenoids.

Therefore, in our approach we used enantiopure (3*S*,3′*S*)-astaxanthin (AXT), which provides the chiroptical output (electronic circular dichroism: ECD and resonance Raman optical activity: RROA), in order to investigate and control the processes of delivery of carotenoid molecules into generic nanoparticles and their assembly inside them. Previously, we demonstrated that chiroptical techniques provide unique information on carotenoid aggregation processes in mixed solvents[14–16] and in cells.[17] The efficiency of the formed nanocarriers for carotenoid transport to primary adipocytes was monitored by Raman microscopy. Our results indicate that efficient encapsulation and formation of stable aggregates inside micelles is complicated by the self-assembling of carotenoid molecules outside nanoparticles and that the process of aggregation is significantly controlled by kinetic and not only thermodynamic factors.

For encapsulation, we used a generic carrier system, Pluronic F-127, poly(ethylene oxide)–poly(propylene oxide)–poly(ethylene oxide) (PEO–PPO–PEO), a block copolymer that has a wide range of biomedical applications, including hydrophobic drug delivery.[18] Micelles were formed *via* direct solubilisation (details in the Experimental section in ESI†). To introduce AXT into the system, it was dissolved in DMSO.

As Fig. 1 shows, both the intensity and shape of the ECD signals depend on the concentration of AXT and time from the formation of the system. Independently of the carotenoid concentration (100 μM: Fig. 1 and Fig. S1, ESI† and 10 μM:

[a] *Faculty of Chemistry, Jagiellonian University, Gronostajowa 2, 30-387, Krakow, Poland. E-mail: agnieszka.kaczor@uj.edu.pl*
[b] *Jagiellonian Centre for Experimental Therapeutics, Jagiellonian University, Bobrzynskiego 14, 30-348, Krakow, Poland*

† Electronic supplementary information (ESI) available: Experimental details, UV-vis spectra complementary to ECD spectra presented in the manuscript text, and ECD and UV-vis spectra of AXT (10 μM) in micelles. See DOI: https://doi.org/10.1039/d2cc02649j

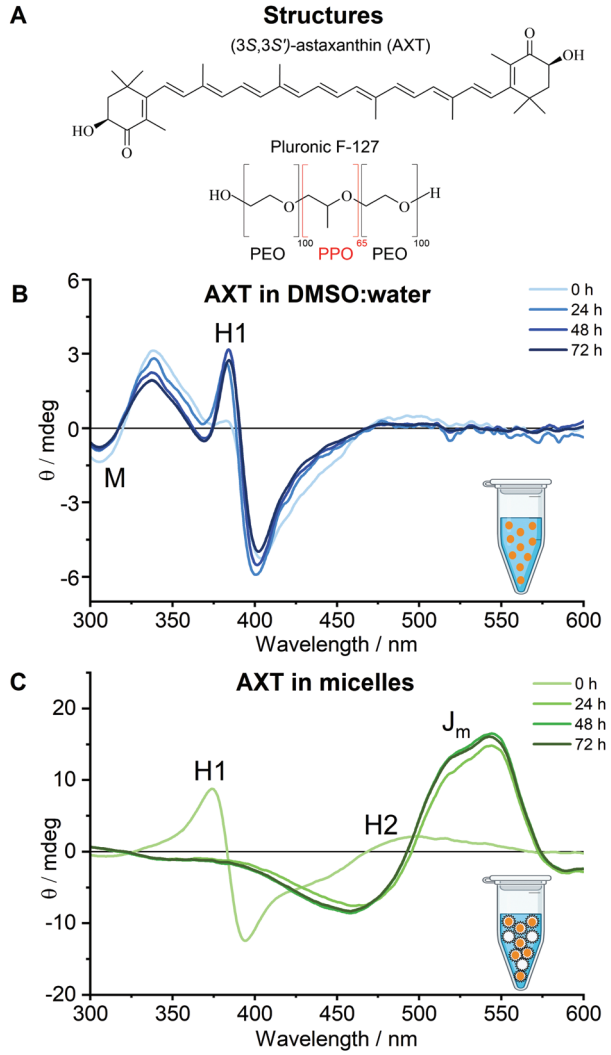

Fig. 1 Molecular structures of AXT, PEO and PPO (A) and ECD spectra of AXT in DMSO : water solution (B, 1 : 49) and AXT in micelles (C: c_{AXT} = 100 μM, c_m = 1 mM) freshly prepared and after stabilization in time.

Fig. S2, ESI†), the ECD spectra of freshly prepared nanocarrier : carotenoid samples show the exciton signal of *H1*-aggregates with the maximum and minimum at *ca.* 374 and 394 and nm, respectively, and traces of the −/+ exciton signal at *ca.* 440 and 490 nm, due to *H2*-assemblies, respectively (Fig. 1C).

Structures and chiroptical spectra of AXT aggregates were previously analyzed in detail.[14,15,19–21] In general, in *H1*-aggregates, xanthophyll molecules, stabilized *via H*-bonds, are tightly ordered in a card-pack manner, for *H2* and *J*-assemblies the supramolecular structure is more relaxed, as shown, among others, by considerably broader ECD bands. The highly dynamic nature of the studied systems is demonstrated by marked spectral changes obtained if the systems are stabilized in time (Fig. 1C). Independently of the carotenoid concentration, after *ca.* 24 h there is a shift in equilibrium toward the formation of aggregates of *J*-type, yet of a different structure than previously observed in mixed solvents[15] as shown by the bathochromic shift of the exciton bands (−/+ exciton signal at *ca.* 460 and 540 nm) (Fig. 1C). The detailed analysis of the signal evolution in time (Fig. S3, ESI†) shows that *J*-aggregates are formed already after 2 hours and their content increases during the 24 hours after system preparation. The signal of *H1*-aggregates formed in DMSO/water solution at the same concentration of DMSO in water does not change with time (Fig. 1B). The general picture that can be drawn is that encapsulated carotenoid molecules are organized into thermodynamically stable *J*-type aggregates within the nanoparticles, but a considerable amount of time is required for the formation of *J*-assemblies inside nanocarriers as it involves either disassembly of *H*-aggregates formed outside nanoparticles and their reassembling inside the micelles or rearrangement of small *H*-aggregates inside the nanocarriers into the *J*-type assemblies.

Resonance enhancement due to exciton coupling of carotenoids in chiral dimers or larger aggregates that have ECD intensity coinciding with the excitation wavelength[14,17,22,23] results in the very intense RROA signal of *J*-aggregates (Fig. 2) that, in agreement with the single-state RROA theory,[24] have the opposite sign to the ECD intensity at 532 nm (the laser excitation wavelength). The RROA bands are negative, but of the same wavenumbers as the Raman signals. Hence *J*-aggregates, but not *H1*-aggregates, provide an RROA signal, and the carotenoid encapsulation can be monitored by RROA in an on/off manner.

To eliminate the formation of kinetically stabilized *H1*-assemblies, the encapsulation was also carried out using a 'feeding strategy', *i.e.*, continuous delivery of the carotenoid in equal and small portions for 3 days to achieve the final AXT concentration of 100 μM. This procedure was implemented to

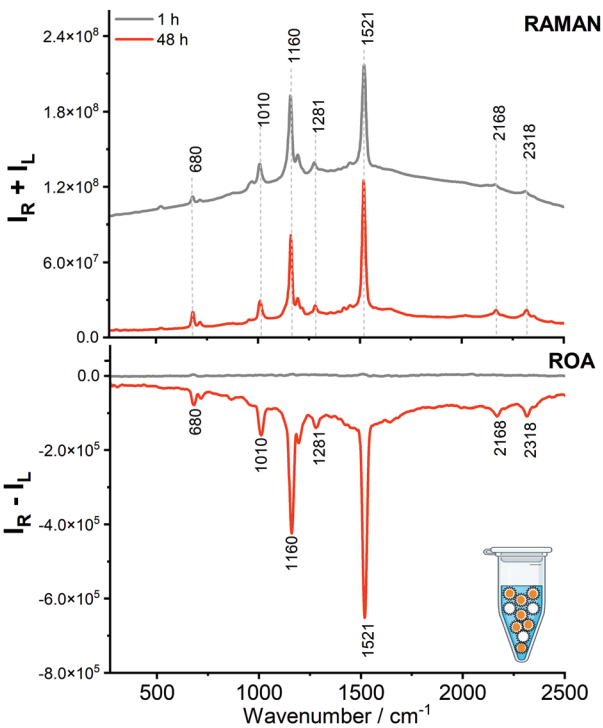

Fig. 2 Resonance Raman and ROA spectra of AXT in micelles (c_{AXT} = 100 μM, c_m = 1 mM).

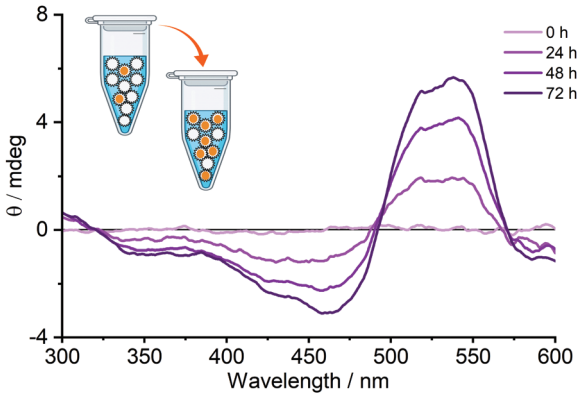

Fig. 3 ECD spectra of AXT in micelles during 'feeding' of nanoparticles with the carotenoid, *i.e.* increasing daily the concentration of AXT up to 100 μM, c_m = 1 mM.

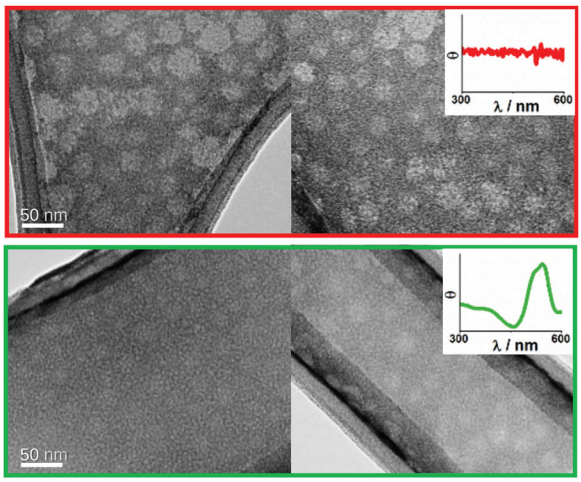

Fig. 4 TEM images of empty micelles (top panel) and AXT in micelles (bottom panel) with the corresponding ECD spectra (insets). For TEM, samples prepared as in Fig. 1 were ten-fold diluted.

decrease the self-aggregation in *H*-assemblies outside micelles and enable systematic encapsulation of the carotenoid in nanoparticles. The obtained spectra (Fig. 3 and Fig. S4, ESI†) show that the formation of the *H*-assemblies is indeed avoided and the recorded ECD *J*-aggregate signal shows a gradual increase with the feeding time (confirmed by anisotropy spectra, Fig. S5, ESI†). The ECD intensity of the system obtained *via* feeding is considerably less intense than the one obtained with micelles formed *de novo* (Fig. 1C), which is the result of the formation of smaller aggregates distributed more evenly between micelles that remain in excess in the system.

The size of the AXT *H*-aggregates does not exceed 200 nm, but the *J*-aggregates are significantly larger and can reach up to 7 μm,[19] and hence can be observed by electron microscopy. The transmission electron microscopy (TEM) images (Fig. 4) confirm that no carotenoid *J*-assemblies outside the micelles are formed and show that nanocarriers with embedded carotenoids are less homogenous in size compared to the empty nanoparticles.

J-aggregates encapsulated in nanocarriers show excellent stability at room temperature (Fig. 5A and Fig. S6A, ESI†). The system is stable for at least 16 days and shows also thermal stability during the Pluronic F127 micelles' phase transition (Fig. 5B and Fig. S6B, ESI†). Interconversion of the soluble form at <30 °C to a liquid crystal form at >30 °C, taking place in the aqueous solution, does not affect the signal of *J*-aggregates up to 60 °C, confirming significant stability of *J*-type carotenoid assemblies embedded in nanocarriers. At temperatures above 37 °C, the rearrangement of *J*-aggregates into a thermodynamically more stable form of *J*-assemblies (J'_m) occurs, as confirmed by the irreversibility of $J_m \rightarrow J'_m$ transition when the system is cooled back to 25 °C.

Resonance Raman and ROA spectra of J'_m and J_m (Fig. S7, ESI†) are very similar as the structure and shape of the chromophore, which gives rise to the resonance, are very similar for both *J*-aggregates.

The main storage place for carotenoids are adipocytes (fat cells) and their concentration is, among other pathologies, reduced in obesity[25] or atherosclerosis.[26] To investigate how

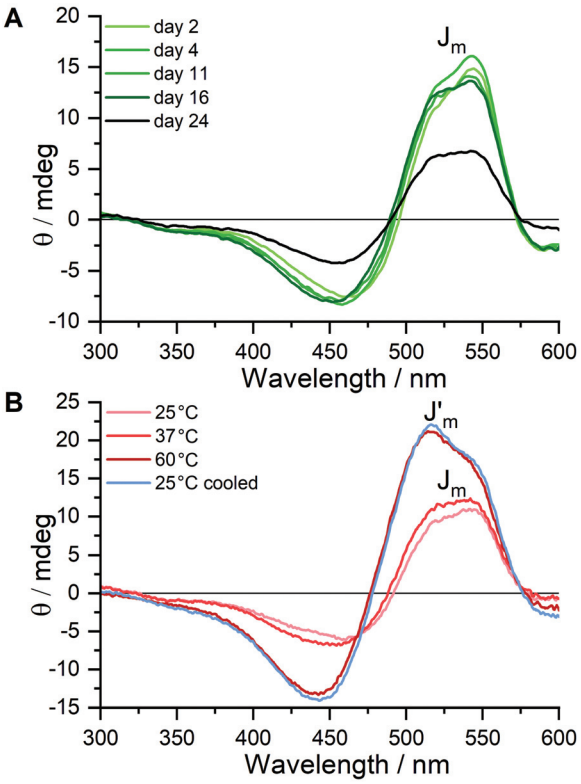

Fig. 5 Stability of *J*-aggregates of AXT in micelles at room temperature (A) and spectral changes due to thermal treatment of the system (B) (c_{AXT} = 100 μM, c_m = 1 mM).

the embedding of carotenoid molecules influences their delivery to cells, the uptake of carotenoid-loaded nanocarriers *via* primary white adipocytes was investigated using high spatial-resolution Raman microscopy (Fig. 6A). The kinetics of delivery of carotenoids embedded in nanocarriers differs considerably

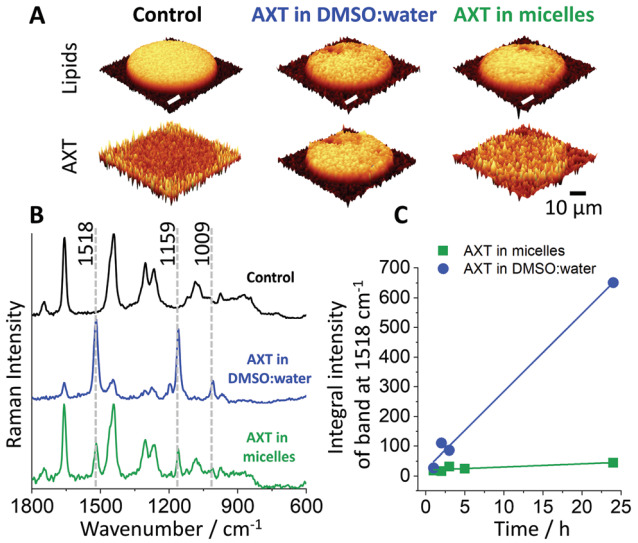

Fig. 6 Primary adipocytes incubated for 24 h without AXT (control, black), with AXT delivered in DMSO:water (blue) and with AXT delivered in micelles (green): the Raman distribution images of the lipids and astaxanthin (A, only the signal inside cells was analyzed) and the average Raman spectra of cells (B) and the kinetics of delivery of carotenoids to adipocytes (C).

compared to the carotenoid dispersion in DMSO-containing medium (Fig. 6B) indicating that nanocarriers provide controlled release of the carotenoid into the cells. Yet, due to slow release, there is a risk that *in vivo* micelles could be eliminated before they deliver the carotenoid into the cells.

In conclusion, the chiroptical output due to enantiopure (3*S*,3′*S*)-astaxanthin enables investigation, in detail, of the carotenoid embedding and self-assembling in Pluronic F-127 nanoparticles.

As demonstrated, the formation of stable carotenoid *J*-assemblies inside the nanocarriers is interfered with by the formation of kinetically stabilized *H*-aggregates outside the micelles, which with time restructure into thermodynamically stable *J*-assemblies embedded in micelles. Moreover, the process of formation of *J*-assemblies is strongly governed by the carotenoid : nanocarrier ratio as shown by the feeding experiment.

Monitoring of the process of the active substance assembling in nanocarriers *via* chiroptical (ECD/RROA) readout can be used to produce tailored-size nanoparticles encapsulating the active substance. In particular, in the studied case, due to the unique selectivity of RROA for the AXT *J*-aggregates, this method guarantees on/off information on *J*-assembly formation. The *J*-aggregates encapsulated in nanocarriers are stable both at room temperature and at the physiological temperature of 37 °C, and provide controlled release of carotenoids to primary murine adipocytes.

Conceptualization – A. K.; methodology – A. O., E. S., K. C., A. W., and A. K.; validation – A. O., E. S., K. C., A. W., and A. K.; investigation – A. O., E. S., K. C., A. and W.; data curation – A. O., E. S., K. C., and A. W.; writing – original draft – A. K.; writing – review and editing – A. O., E. S., K. C., and A. W.; visualization – A. O., E. S., and K. C.; supervision – A. K.; project administration – A. K.; funding acquisition – A. K.

This work was supported by the National Science Centre Poland (projects 2019/33/B/ST4/00878 and 2020/37/B/ST4/01168 to A. K.).

Conflicts of interest

There are no conflicts to declare.

References

1 A. H. Eliassen, X. Liao, B. Rosner, R. M. Tamimi, S. S. Tworoger and S. E. Hankinson, *Am. J. Clin. Nutr.*, 2015, **101**, 1197–1205.
2 C. N. Holick, D. S. Michaud, R. Stolzenberg-Solomon, S. T. Mayne, P. Pietinen, P. R. Taylor, J. Virtamo and D. Albanes, *Am. J. Epidemiol.*, 2002, **156**, 536–547.
3 Y. Ito, M. Kurata, K. Suzuki, N. Hamajima, H. Hishida and K. Aoki, *J. Epidemiol.*, 2006, **16**, 154–160.
4 S. Mukherjee and J. W. Yun, *Phytomedicine*, 2022, 96.
5 B. Zhao, M. Liu, H. Liu, J. Xie, J. Yan, X. Hou and J. Liu, *Food Funct.*, 2021, **12**, 6283–6293.
6 A. Bartelt and J. Heeren, *Nat. Rev. Endocrinol.*, 2014, **10**, 24–36.
7 K. Canene-Adams and J. W. Erdman, in *Carotenoids: Volume 5: Nutrition and Health*, ed. G. Britton, H. Pfander and S. Liaaen-Jensen, Birkhäuser Basel; Basel, 2009, DOI: 10.1007/978-3-7643-7501-0_7, pp. 115–148.
8 D. Fu, S. Deng, D. J. McClements, L. Zhou, L. Zou, J. Yi, C. Liu and W. Liu, *Food Hydrocolloids*, 2019, **89**, 80–89.
9 C. Liu, S. Zhang, D. J. McClements, D. Wang and Y. Xu, *J. Agric. Food Chem.*, 2019, **67**, 5113–5121.
10 A. K. D. O. C. Medeiros, C. D. C. Gomes, M. L. Q. D. A. Amaral, L. D. G. D. Medeiros, I. Medeiros, D. L. Porto, C. F. S. Aragão, B. L. L. Maciel, A. H. D. A. Morais and T. S. Passos, *Food Chem.*, 2019, **270**, 562–572.
11 L. Salvia-Trujillo, C. Qian, O. Martín-Belloso and D. J. McClements, *Food Chem.*, 2013, **141**, 1472–1480.
12 J. Weiss, E. A. Decker, D. J. McClements, K. Kristbergsson, T. Helgason and T. Awad, *Food Biophys.*, 2008, **3**, 146–154.
13 D. Horn and J. Rieger, *Angew. Chem., Int. Ed.*, 2001, **40**, 4330–4361.
14 M. Dudek, G. Zajac, A. Kaczor and M. Baranska, *J. Phys. Chem. B*, 2016, **120**, 7807–7814.
15 G. Zajac, A. Kaczor, A. Pallares Zazo, J. Mlynarski, M. Dudek and M. Baranska, *J. Phys. Chem. B*, 2016, **120**, 4028–4033.
16 G. Zajac, E. Machalska, A. Kaczor, J. Kessler, P. Bouř and M. Baranska, *Phys. Chem. Chem. Phys.*, 2018, **20**, 18038–18046.
17 M. Dudek, E. Machalska, T. Oleszkiewicz, E. Grzebelus, R. Baranski, P. Szcześniak, J. Mlynarski, G. Zajac, A. Kaczor and M. Baranska, *Angew. Chem., Int. Ed.*, 2019, **58**, 8383–8388.
18 M. S. H. Akash and K. Rehman, *J. Controlled Release*, 2015, **209**, 120–138.
19 S. Köhn, H. Kolbe, M. Korger, C. Köpsel, B. Mayer, H. Auweter, E. Lüddecke, H. Bettermann and H.-D. Martin, in *Carotenoids: Natural Functions*, ed. G. Britton, S. Liaaen-Jensen and H. Pfander, Birkhäuser Basel; Basel, Volume 4, 2008, DOI: 10.1007/978-3-7643-7499-0_5, pp. 53–98.
20 A. J. Musser, M. Maiuri, D. Brida, G. Cerullo, R. H. Friend and J. Clark, *J. Am. Chem. Soc.*, 2015, **137**, 5130–5139.
21 F. C. Spano, *J. Am. Chem. Soc.*, 2009, **131**, 4267–4278.
22 T. Fujisawa, R. L. Leverenz, M. Nagamine, C. A. Kerfeld and M. Unno, *J. Am. Chem. Soc.*, 2017, **139**, 10456–10460.
23 S. Haraguchi, M. Hara, T. Shingae, M. Kumauchi, W. D. Hoff and M. Unno, *Angew. Chem., Int. Ed.*, 2015, **54**, 11555–11558.
24 L. A. Nafie, *Chem. Phys.*, 1996, **205**, 309–322.
25 M. Östh, A. Öst, P. Kjolhede and P. Strålfors, *PLoS One*, 2014, **9**, e85610.
26 Z. Majka, K. Czamara, P. Wegrzyn, R. Litwinowicz, J. Janus, S. Chlopicki and A. Kaczor, *Analyst*, 2021, **146**, 270–276.